Chemical Science

EDGE ARTICLE

View Article Online
View Journal

Cite this: DOI: 10.1039/c3sc52789a

High-capacity Li_2S–graphene oxide composite cathodes with stable cycling performance†

Zhi Wei Seh,[a] Haotian Wang,[b] Nian Liu,[c] Guangyuan Zheng,[d] Weiyang Li,[a] Hongbin Yao[a] and Yi Cui*[ae]

Received 7th October 2013
Accepted 9th December 2013

DOI: 10.1039/c3sc52789a

www.rsc.org/chemicalscience

With its high theoretical capacity of 1166 mA h g^{-1}, Li_2S is a promising prelithiated cathode material for applications such as vehicle electrification and grid energy storage. Herein, we demonstrate facile synthesis of Li_2S–graphene oxide composites for use as high-capacity and stable-cycling Li_2S cathodes. The wrapping of graphene oxide onto the surface of Li_2S through favorable lithium–oxygen interactions helps to minimize the dissolution of intermediate polysulfides into the electrolyte during cycling, which is a major reason for rapid capacity decay. Using the Li_2S–graphene oxide composites as a cathode material, we demonstrate a high discharge capacity of 782 mA h g^{-1} of Li_2S (~1122 mA h g^{-1} of S) with stable cycling performance over 150 charge–discharge cycles.

Introduction

There is currently a great deal of interest in the development of rechargeable batteries with high energy density and long cycle life for vehicle electrification and grid energy storage applications.[1–6] Although rechargeable lithium-ion batteries are widely used today in consumer devices, their energy density is too low to render them viable for the above-mentioned applications.[1–6] The major limiting factor in lithium-ion batteries today is the low theoretical capacity of conventional intercalation cathodes based on transition metal oxides and phosphates.[1–6] On the other hand, Li_2S is a promising cathode material with a high theoretical capacity of 1166 mA h g^{-1} ($8Li_2S \leftrightarrow S_8 + 16Li$), which is ~4 times that of its transition metal oxide or phosphate counterparts.[7–14] Unlike sulfur cathodes, Li_2S is in a fully-lithiated state and can be paired with lithium metal-free anodes (such as silicon and tin), thus obviating the safety concerns and dendrite formation associated with lithium metal.[7–14] Moreover, the fact that Li_2S undergoes volumetric contraction in the initial delithiation process (instead of expansion as in the case of sulfur cathodes) leads to less structural damage to the entire electrode.[11] Although sulfur cathodes are now under intensive study,[15–35] the potential of using Li_2S as a starting cathode material has not received adequate attention. Similar to their sulfur counterparts, Li_2S cathodes are plagued with the problems of low electronic and ionic conductivity as well as the dissolution of intermediate lithium polysulfide species (Li_2S_n) into the electrolyte, leading to rapid capacity decay and low Coulombic efficiency.[7–14] Wrapping of Li_2S with mesoporous carbon or carbon black has been the most common strategy used to constrain Li_2S_n species and reduce their dissolution into the electrolyte,[7–13] though the resulting cycling performance still leaves much room for improvement. This is probably because carbon, being largely non-polar in nature, does not interact favorably with the polar Li_2S and intermediate Li_2S_n species involved in the cycling process.

Previous *ab initio* simulations have shown that oxygenated functional groups can bind strongly with Li_2S and Li_2S_n species through Li–O interactions.[12] Inspired by these theoretical simulations, herein we demonstrate experimentally the use of mildly-oxidized graphene oxide (GO) as an encapsulation material for Li_2S cathodes (Fig. 1a). The wrapping of GO onto the surface of Li_2S through favorable Li–O interactions helps to minimize the dissolution of intermediate Li_2S_n species into the electrolyte during cycling, which is a major reason for rapid capacity decay. Using the Li_2S–GO composites as a cathode material, we demonstrate a high discharge capacity of 782 mA h g^{-1} of Li_2S (~1122 mA h g^{-1} of S) and stable cycling performance over 150 charge–discharge cycles.

Results and discussion

First, mildly-oxidized GO was synthesized using the modified Hummer's method[20,36] (ESI,† Fig. S1) and then re-dispersed into anhydrous ethyl acetate. Micron-sized commercial Li_2S

[a]Department of Materials Science and Engineering, Stanford University, Stanford, California 94305, USA. E-mail: yicui@stanford.edu
[b]Department of Applied Physics, Stanford University, Stanford, California 94305, USA
[c]Department of Chemistry, Stanford University, Stanford, California 94305, USA
[d]Department of Chemical Engineering, Stanford University, Stanford, California 94305, USA
[e]Stanford Institute for Materials and Energy Science, SLAC National Accelerator Laboratory, Menlo Park, California 94025, USA

† Electronic supplementary information (ESI) available: Details of materials synthesis, characterization, electrochemical measurements, electrolyte testing, Table S1 and Fig. S1–S4. See DOI: 10.1039/c3sc52789a

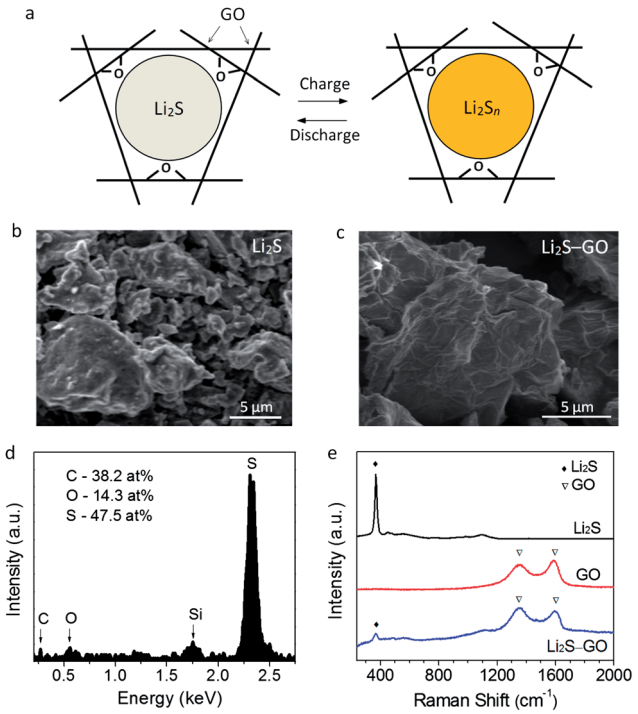

Fig. 1 (a) Schematic showing the wrapping of Li_2S with GO and the favorable interactions between oxygenated groups in GO and polar Li_2S and Li_2S_n species involved in the cycling process. (b and c) SEM images of (b) commercial Li_2S particles and (c) as-synthesized Li_2S–GO composites. (d) EDX spectrum of the Li_2S–GO composites, showing the presence and relative atomic fractions of C, O and S (Li cannot be detected using EDX; the Si peak arises due to the use of a Si substrate). (e) Raman spectra of pristine Li_2S, pristine GO and Li_2S–GO composites.

particles were then added (Li_2S : GO = 75 : 25 by weight) followed by ultrasonication and stirring to allow wrapping of GO onto the surface of Li_2S. Fig. 1b and c show scanning electron microscopy (SEM) images of the Li_2S particles before and after GO coating. We can see that the surface of the Li_2S particles changes to a more sheet-like appearance after GO coating (Fig. 1c; see also ESI,† Fig. S2 for a low-magnification SEM image). Energy-dispersive X-ray spectroscopy (EDX) analysis in Fig. 1d shows the presence of S, C and O in the Li_2S–GO composites (Li cannot be detected using EDX; the Si peak arises due to the use of a Si substrate). From the relative atomic fractions of the various elements, the Li_2S content in the composite was determined to be ~76 wt% (ESI,† Table S1), which is consistent with the relative amounts of Li_2S and GO added during the synthesis (75 : 25 by weight). The surface coating of GO on the Li_2S particles was further confirmed using Raman spectroscopy. We see that the Raman spectrum of pristine Li_2S shows the characteristic T_{2g} phonon mode of Li_2S at 372 cm^{-1} corresponding to Li–S bond vibrations,[37,38] while that of GO shows the characteristic D and G bands at 1350 and 1590 cm^{-1}, respectively (Fig. 1e).[39] The Raman spectrum of the Li_2S–GO composites shows both the peaks of Li_2S and GO, though the intensity of the Li_2S T_{2g} peak is much weaker compared to GO (Fig. 1e). Since Raman spectroscopy is a surface-sensitive technique, this observation indicates that the surface of the Li_2S particles has been largely covered with GO, consistent with the SEM image in Fig. 1c.

Previous *ab initio* simulations have shown that oxygenated functional groups can bind strongly with Li_2S through coordination-like interactions between the lone pairs on electronegative O and the Li in Li_2S.[12] In Fig. 2a, we show a schematic depicting an example of such a Li–O interaction between Li_2S and epoxide groups commonly found in GO. To verify the presence of such Li–O interactions in the Li_2S–GO composites, we performed X-ray photoelectron spectroscopy (XPS) and Raman spectroscopy measurements, which are known to be very sensitive to the chemical environment. To prevent moisture contamination of Li_2S, special precautions were taken during characterization (see ESI† for details). We see that the Li 1s XPS spectrum of pristine Li_2S can be fitted with a single peak with a binding energy of 54.6 eV (Fig. 2b), which corresponds to Li in the Li–S bond.[40] In contrast, the Li 1s spectrum of the Li_2S–GO composites shows asymmetric broadening towards a higher binding energy (Fig. 2b), which indicates a change in the chemical environment experienced by Li. This spectrum can be fitted using 2 peaks: the peak at 54.6 eV corresponds to Li in the Li–S bond, while the additional peak at 55.4 eV can be attributed to Li–O interaction in the Li_2S–GO composites in accordance with tabulated values.[40]

This is further supported by close analysis of the T_{2g} Raman peak of Li_2S in the pristine Li_2S and Li_2S–GO composite samples. The T_{2g} Raman peak of pristine Li_2S occurs at 372 cm^{-1} (Fig. 2c), consistent with values in the literature.[37,38] We see a red-shift in the Raman peak position from 372 cm^{-1} in pristine Li_2S to 369 cm^{-1} in the Li_2S–GO composites (Fig. 2c) which indicates a change in chemical environment. Since the T_{2g} phonon mode in Li_2S arises due to Li–S bond vibrations,[37,38] a red-shift (decrease in frequency) indicates a decrease in the force constant and slight weakening of the Li–S bonds in the

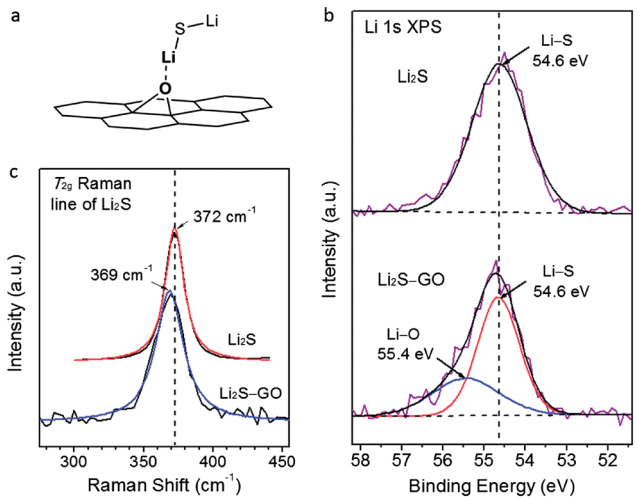

Fig. 2 (a) Schematic showing an example of Li–O interaction between Li_2S and epoxide groups commonly found in GO. (b) XPS spectra of the Li 1s peak and (c) Raman spectra of the T_{2g} phonon mode of Li_2S in pristine Li_2S and Li_2S–GO composites, together with their respective fitted peaks.

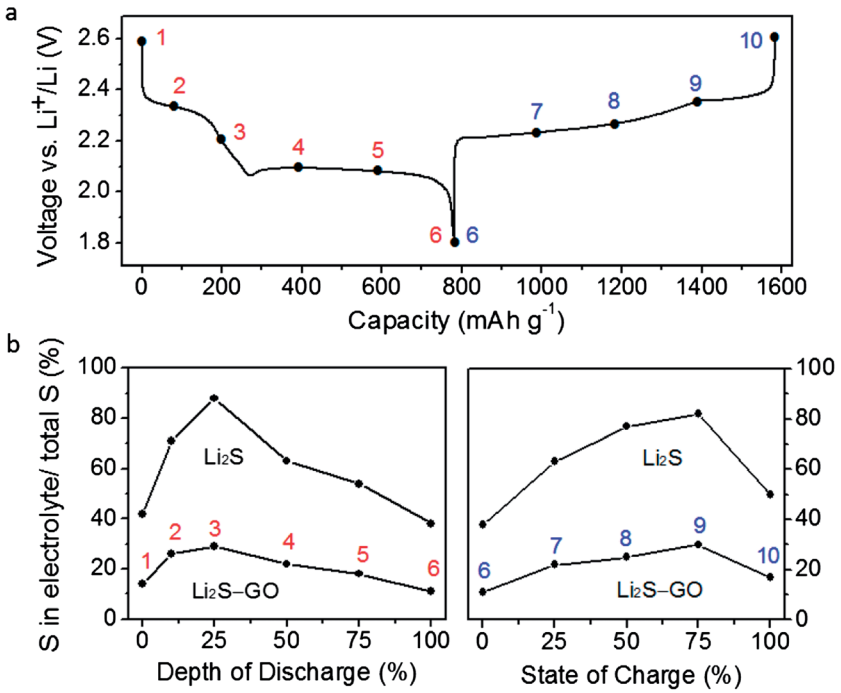

Fig. 3 (a) Typical discharge and charge voltage profile showing various depths of discharge and states of charge (points 1 to 10) and (b) the corresponding percentage of sulfur measured in the electrolyte relative to the total sulfur mass on the electrode at these various points for Li_2S–GO and pristine Li_2S cathodes. Specific capacity values were calculated based on the mass of Li_2S.

Li_2S–GO composites.[41,42] This can be explained by the strongly-electronegative O atoms in GO interacting with Li in Li_2S, causing the electron density along the Li–S bonds in Li_2S to be diminished and the bonds to be weakened, as evidenced by Raman spectroscopy.

It is well-known that dissolution of intermediate Li_2S_n species into the electrolyte is a major reason for rapid capacity decay in Li_2S cathodes.[7–14] Previous *ab initio* simulations have shown that oxygenated functional groups (such as those found on GO) can bind strongly with Li_2S_n species as well,[12] which would enable GO to constrain these polysulfide species during cycling. To verify this, working electrodes were prepared by mixing the Li_2S–GO composites with carbon black and binder (70 : 25 : 5 by weight) in *N*-methyl-2-pyrrolidinone to form a

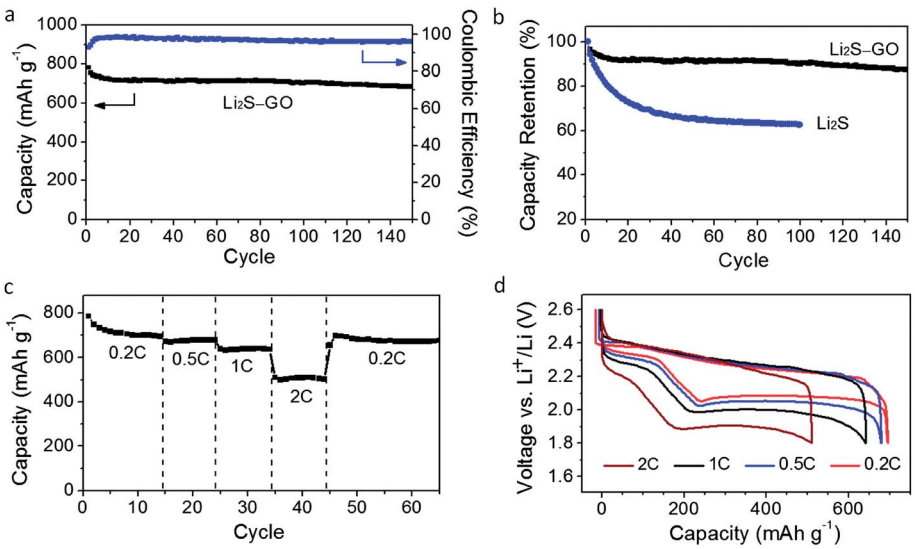

Fig. 4 (a) Specific capacity and Coulombic efficiency of Li_2S–GO composite cathodes over 150 cycles at 0.2 C. (b) Capacity retention of Li_2S–GO composite cathodes cycled at 0.2 C in comparison with pristine Li_2S cathodes. (c) Specific capacity and (d) voltage profiles of Li_2S–GO composite cathodes cycled at various C-rates from 0.2 C to 2 C. Specific capacity values were calculated based on the mass of Li_2S.

slurry, which was then coated onto aluminum foil and dried in a glove box. The typical mass loading of Li_2S was ~1 mg cm^{-2}. 2032-type coin cells were then assembled with lithium foil as the counter electrode. Pristine Li_2S cathodes were also prepared in the same way for comparison. The cathodes were first activated at C/20 (1 C = 1166 mA g^{-1}) by charging to a high cutoff voltage of 3.8 V *vs.* Li^+/Li to overcome the initial potential barrier associated with micron-sized Li_2S particles (ESI,† Fig. S3).[11] The cathodes were then subject to a discharge–charge cycle, during which the electrolyte was tested for sulfur content using inductively coupled plasma-optical emission spectroscopy (ICP-OES) at various intermediate stages (see ESI† for details). Points 1 to 10 in Fig. 3a correspond to various depths of discharge (DOD) and states of charge (SOC) during cycling, where 100% DOD (point 6) and 100% SOC (point 10) refer to the maximum discharge and charge capacities attained, respectively. The ICP-OES results showed significantly lower percentage dissolution of sulfur into the electrolyte during cycling for the Li_2S–GO composites compared to pristine Li_2S cathodes (Fig. 3b). At point 3 during the discharge process (25% DOD), we measured a maximum of 29% of the total sulfur mass on the electrode dissolved into the electrolyte for the Li_2S–GO composites, compared to 88% in the case of pristine Li_2S cathodes (Fig. 3b). Similarly, at point 9 during the charge process (75% SOC), 30% dissolution of the total sulfur mass into the electrolyte was measured for the Li_2S–GO composites, compared to 82% in the case of pristine Li_2S cathodes (Fig. 3b). This indicates the effectiveness of the GO wrapping in constraining Li_2S_n species, hence reducing their loss into the electrolyte during cycling.

To further evaluate their electrochemical performance, the Li_2S–GO composite and pristine Li_2S cathodes were cycled galvanostatically from 1.8–2.6 V *vs.* Li^+/Li. Specific capacity values were calculated based on the mass of Li_2S. From Fig. 4a, we see that the Li_2S–GO composite cathodes showed stable cycling at 0.2 C with a high initial capacity of 782 mA h g^{-1} of Li_2S (theoretical capacity 1166 mA h g^{-1}). The capacity retentions achieved at the end of 50, 100 and 150 cycles were 92%, 90% and 88% respectively, relative to the initial cycle (Fig. 4b). The average Coulombic efficiency over the 150 cycles was calculated to be 97% (Fig. 4a). In comparison, pristine Li_2S cathodes exhibited greater capacity decay under identical testing conditions (Fig. 4b). The capacity retention of the pristine Li_2S cathodes was only 62% after 100 cycles (compared to 90% for Li_2S–GO composites), indicating a greater degree of polysulfide dissolution into the electrolyte in the former case. The stable cycling performance of the Li_2S–GO composite provides further evidence for the role of GO wrapping in constraining Li_2S_n species during the cycling process.

Next, the Li_2S–GO composite cathodes were cycled at different C-rates to evaluate their rate capability and electrode kinetics (Fig. 4c and d). When the C-rate was increased successively from 0.2 C to 0.5 C to 1 C, the cells delivered high stabilized capacities of 695, 680 and 640 mA h g^{-1} of Li_2S respectively (Fig. 4c). The capacities achieved at 0.5 C and 1 C correspond to 98% and 92% of the capacity that was attained at 0.2 C, indicating good reaction kinetics in the cathodes. Even at a C-rate of 2 C, a reversible capacity of 510 mA h g^{-1} of Li_2S could be attained. When the C-rate was switched abruptly from 2 C back to 0.2 C again, the original capacity was mostly recovered (Fig. 4c), indicating the robustness and stability of the cathode material. The morphology of the Li_2S–GO composite cathodes was also examined after 150 cycles at 0.2 C. At the end of 150 cycles, the voltage was maintained at 1.8 V *vs.* Li^+/Li for over 20 h and the cell was disassembled in the discharged state. We see that the surface of the Li_2S particles retain their sheet-like appearance after cycling (ESI,† Fig. S4), which indicates that the GO wrapping is intact and effective in constraining intermediate polysulfides to reduce their dissolution into the electrolyte during cycling. As a result, the solid Li_2S formed at the end of discharge does not precipitate randomly and irregularly all over the electrode and the original morphology is largely preserved. Finally, we note that during the cycling process, when Li_2S is converted to S_8 at the fully-charged state, the strong C–S and O–S interactions between S_8 and GO will help to immobilize the S_8 species and stabilize the electrode, contributing to the stable cycling performance as well.[21]

Conclusion

We have demonstrated the facile synthesis of high-performance Li_2S–GO composite cathodes in which the wrapping of GO onto the surface of Li_2S through favorable Li–O interactions helps to constrain intermediate Li_2S_n species during cycling, hence resulting in stable cycling performance. Further work is currently ongoing to pair these stable-cycling Li_2S–GO composite cathodes with lithium metal-free anodes (such as silicon or tin) to achieve a full-cell configuration. This work provides insight on the use of suitable encapsulation materials that bind strongly with Li_2S cathodes, for the future development of high-capacity and long-lasting rechargeable batteries.

Acknowledgements

This work was supported as part of the Joint Center for Energy Storage Research (JCESR), an Energy Innovation Hub funded by the US Department of Energy, Office of Science, Basic Energy Sciences. Z.W.S. and G.Z. acknowledge the support of an A*STAR National Science Scholarship.

References

1 B. Kang and G. Ceder, *Nature*, 2009, **458**, 190–193.
2 Y.-M. Chiang, *Science*, 2010, **330**, 1485–1486.
3 M. S. Whittingham, *Chem. Rev.*, 2004, **104**, 4271–4301.
4 J. B. Goodenough and K.-S. Park, *J. Am. Chem. Soc.*, 2013, **135**, 1167–1176.
5 K. Kang, K. Song, H. Heo, S. Yoo, G. S. Kim, G. Lee, Y. M. Kang and M. H. Jo, *Chem. Sci.*, 2011, **2**, 1090–1093.
6 P. G. Bruce, S. A. Freunberger, L. J. Hardwick and J.-M. Tarascon, *Nat. Mater.*, 2012, **11**, 19–29.
7 J. Hassoun and B. Scrosati, *Angew. Chem., Int. Ed.*, 2010, **49**, 2371–2374.
8 M. Nagao, A. Hayashi and M. Tatsumisago, *J. Mater. Chem.*, 2012, **22**, 10015–10020.

9 K. Cai, M.-K. Song, E. J. Cairns and Y. Zhang, *Nano Lett.*, 2012, **12**, 6474–6479.
10 Y. Yang, M. T. McDowell, A. Jackson, J. J. Cha, S. S. Hong and Y. Cui, *Nano Lett.*, 2010, **10**, 1486–1491.
11 Y. Yang, G. Zheng, S. Misra, J. Nelson, M. F. Toney and Y. Cui, *J. Am. Chem. Soc.*, 2012, **134**, 15387–15394.
12 Z. W. Seh, Q. Zhang, W. Li, G. Zheng, H. Yao and Y. Cui, *Chem. Sci.*, 2013, **4**, 3673–3677.
13 J. Guo, Z. Yang, Y. Yu, H. D. Abruna and L. A. Archer, *J. Am. Chem. Soc.*, 2013, **135**, 763–767.
14 Z. Lin, Z. Liu, N. J. Dudney and C. Liang, *ACS Nano*, 2013, **7**, 2829–2833.
15 H. Yamin, A. Gorenshtein, J. Penciner, Y. Sternberg and E. Peled, *J. Electrochem. Soc.*, 1988, **135**, 1045–1048.
16 X. M. He, W. H. Pu, J. G. Ren, L. Wang, J. L. Wang, C. Y. Jiang and C. R. Wan, *Electrochim. Acta*, 2007, **52**, 7372–7376.
17 X. Ji, K. T. Lee and L. F. Nazar, *Nat. Mater.*, 2009, **8**, 500–506.
18 X. Ji, S. Evers, R. Black and L. F. Nazar, *Nat. Commun.*, 2011, **2**, 325.
19 J. Schuster, G. He, B. Mandlmeier, T. Yim, K. T. Lee, T. Bein and L. F. Nazar, *Angew. Chem., Int. Ed.*, 2012, **51**, 3591–3595.
20 H. Wang, Y. Yang, Y. Liang, J. T. Robinson, Y. Li, A. Jackson, Y. Cui and H. Dai, *Nano Lett.*, 2011, **11**, 2644–2647.
21 L. Ji, M. Rao, H. Zheng, L. Zhang, Y. Li, W. Duan, J. Guo, E. J. Cairns and Y. Zhang, *J. Am. Chem. Soc.*, 2011, **133**, 18522–18525.
22 B. Zhang, X. Qin, G. R. Li and X. P. Gao, *Energy Environ. Sci.*, 2010, **3**, 1531–1537.
23 N. Jayaprakash, J. Shen, S. S. Moganty, A. Corona and L. A. Archer, *Angew. Chem., Int. Ed.*, 2011, **50**, 5904–5908.
24 R. Elazari, G. Salitra, A. Garsuch, A. Panchenko and D. Aurbach, *Adv. Mater.*, 2011, **23**, 5641–5644.
25 S. Xin, L. Gu, N.-H. Zhao, Y.-X. Yin, L.-J. Zhou, Y.-G. Guo and L.-J. Wan, *J. Am. Chem. Soc.*, 2012, **134**, 18510–18513.
26 Z. Lin, Z. Liu, W. Fu, N. J. Dudney and C. Liang, *Angew. Chem., Int. Ed.*, 2013, **52**, 7460–7463.
27 L. Xiao, Y. Cao, J. Xiao, B. Schwenzer, M. H. Engelhard, L. V. Saraf, Z. Nie, G. J. Exarhos and J. Liu, *Adv. Mater.*, 2012, **24**, 1176–1181.
28 Y. Cao, X. Li, I. A. Aksay, J. Lemmon, Z. Nie, Z. Yang and J. Liu, *Phys. Chem. Chem. Phys.*, 2011, **13**, 7660–7665.
29 T. H. Hwang, D. S. Jung, J.-S. Kim, B. G. Kim and J. W. Choi, *Nano Lett.*, 2013, **13**, 4532–4538.
30 S. Moon, Y. H. Jung, W. K. Jung, D. S. Jung, J. W. Choi and D. K. Kim, *Adv. Mater.*, 2013, **25**, 6547–6553.
31 Y. Fu, Y.-S. Su and A. Manthiram, *Angew. Chem., Int. Ed.*, 2013, **52**, 6930–6935.
32 Y.-S. Su and A. Manthiram, *Nat. Commun.*, 2012, **3**, 1166.
33 L. Suo, Y.-S. Hu, H. Li, M. Armand and L. Chen, *Nat. Commun.*, 2013, **4**, 1481.
34 Z. W. Seh, W. Li, J. J. Cha, G. Zheng, Y. Yang, M. T. McDowell, P.-C. Hsu and Y. Cui, *Nat. Commun.*, 2013, **4**, 1331.
35 W. Li, G. Zheng, Y. Yang, Z. W. Seh, N. Liu and Y. Cui, *Proc. Natl. Acad. Sci. U. S. A.*, 2013, **110**, 7148–7153.
36 W. S. Hummers and R. E. Offeman, *J. Am. Chem. Soc.*, 1958, **80**, 1339–1339.
37 B. Bertheville, H. Bill and H. Hagemann, *J. Phys.: Condens. Matter*, 1998, **10**, 2155–2169.
38 A. Grzechnik, A. Vegas, K. Syassen, I. Loa, M. Hanfland and M. Jansen, *J. Solid State Chem.*, 2000, **154**, 603–611.
39 D. C. Marcano, D. V. Kosynkin, J. M. Berlin, A. Sinitskii, Z. Sun, A. Slesarev, L. B. Alemany, W. Lu and J. M. Tour, *ACS Nano*, 2010, **4**, 4806–4814.
40 J. F. Moulder and J. Chastain, *Handbook of X-ray photoelectron spectroscopy: a reference book of standard spectra for identification and interpretation of XPS data*, Physical Electronics Division, Perkin-Elmer Corp, 1995.
41 C. Q. Sun, L. K. Pan, C. M. Li and S. Li, *Phys. Rev. B: Condens. Matter Mater. Phys.*, 2005, **72**, 134301.
42 M. X. Gu, L. K. Pan, B. K. Tay and C. Q. Sun, *J. Raman Spectrosc.*, 2007, **38**, 780–788.